COMPUTATIONAL MECHANICS 2023
38th conference with international participation
Srní
October 23 - 25, 2023

# Uncertainties in gear mesh excitation of electric drives

K. Dráždil[a,c], J. Otta[b]

[a]ZF Engineering Plzeň s.r.o., Univerzitní HQ Plant, Univerzitní 1159/53, 301 00 Plzeň, Czech Republic
[b]ZF Friedrichshafen AG, 88038 Friedrichshafen, Germany
[c]Department of Mechanics, Faculty of Applied Sciences, University of West Bohemia, Univerzitní 8, 301 00 Plzeň, Czech Republic

## 1. Introduction

Nowadays, virtual validation enhances development by digitally testing products, reducing physical prototypes, and accelerating time-to-market, while also considering uncertainties from manufacturing and assembling, which are essential for ensuring real-world reliability and performance.

This paper investigates the impact of uncertainties on flank line deviations in gears and their influence on the vibroacoustic system response used in an electric drive simulation. The overall system's response is based on multi-stage toolchain including non-linear quasi-static finite element (FE) analysis, gear mesh simulation, and linear dynamic FE analysis in the frequency domain, as depicted in Fig. 1.

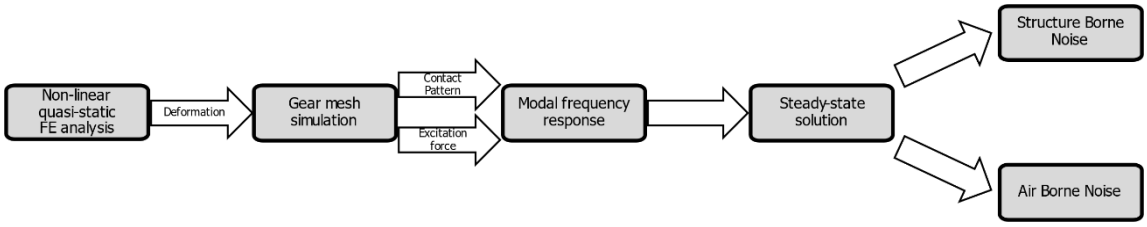


Fig. 1. Simulation toolchain

This representation is better for parametric studies and offers a significant speed advantage over the traditional time-domain representation in Multi-Body System.

## 2. Simulation toolchain

The current approach relies on comprehensive FE models of the electric drive system containing components like housings, electric motor, drive shafts, gears, bearings, and other relevant internal parts, as depicted in Fig. 2. This modelling enables a precise representation of mass and stiffness distribution, along with the dynamic interactions between the electric motor and the transmission.

### *2.1 Non-linear quasi-static finite element (FE) analysis*

The nonlinear quasi-static problem described by

$$\mathbf{K}(\mathbf{x},\mathbf{p})\mathbf{x} = \mathbf{f}(\mathbf{p}), \tag{1}$$

where the stiffness matrix $\mathbf{K}(\mathbf{x},\mathbf{p})$ is dependent on the response vector $\mathbf{x}$ and on the vector of parameters $\mathbf{p}$ as well as the excitation force vector $\mathbf{f}(\mathbf{p})$, can be solved by any of commercial solvers. The vector of parameters $\mathbf{p}$ expressing uncertainties can be decomposed into structural parameters $\mathbf{p}_S$ resulting from design factors such as assembling tolerances and imperfections,

as well as excitation parameters $\mathbf{p_E}(\mathbf{p_S})$ arising from gear mesh interactions (interdependence of excitation and structure), i.e. $\mathbf{p} = [\mathbf{p_S} \quad \mathbf{p_E}(\mathbf{p_S})]$.

The flank line deviations $\mathbf{x_{FLD}}$ resulting from the deformation of the internal components under the loading conditions are visually depicted in Fig. 3. These deviations can be formulated as a function of the local deflections of gears $\mathbf{x_{r1}}, \mathbf{x_{r2}}$, which contribute to the deformation within the gear mesh

$$\mathbf{x_{FLD}}(\mathbf{p_S}) = \mathbf{x_{FLD}}(\mathbf{x_{r1}}(\mathbf{p_S}), \mathbf{x_{r2}}(\mathbf{p_S})). \tag{2}$$

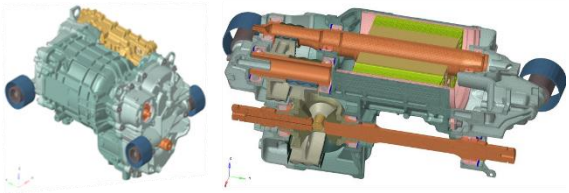

Fig. 2. (a) FE model of electric drive
(b) Section cut of the FE model

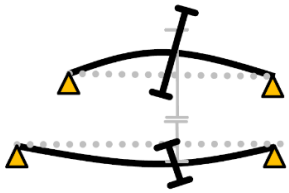

Fig. 3. Gear misalignment

*2.2 Gear mesh simulation*

Having laid the foundation for analysing the local deformations of the gears in the earlier section, the assessment of the gear mesh follows to derive the gear mesh forces essential for subsequent vibroacoustic simulations.

Gear mesh excitation forces are dependent on local deflections of gears causing gear mesh errors contributing to the continuous periodic transmission error (TE), as illustrated in Fig. 4.

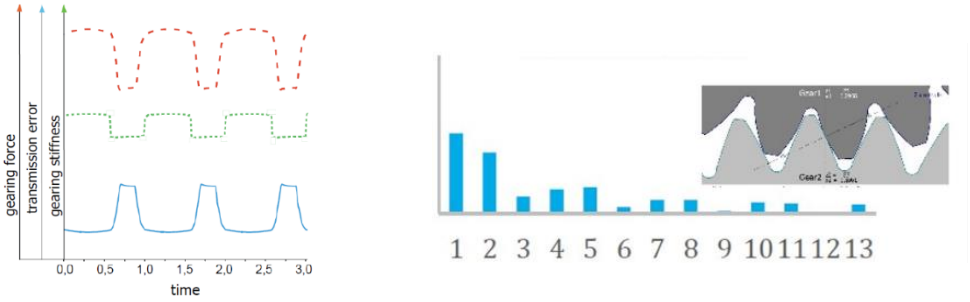


Fig. 4. (a) Example of periodic gear mesh excitation (b) Fourier coefficients

Subsequently, the continuous periodic gear mesh force $\mathbf{f_G}(\mathbf{p}, t)$ can be approximated by partial sum of its expansion into a Fourier series, with each term corresponding to the excitation orders originating from the gear mesh [2] as

$$\mathbf{f_G}(\mathbf{p}, t) \cong \sum_{k=1}^{N} c_{zk}(\mathbf{p}, t)\left[x_M + x_{fk}(\mathbf{p}, t)\right] \cong \sum_{k=0}^{N} F_k^G(\mathbf{p}) \cos(k\omega t), \tag{3}$$

where $c_{zk}(t)$ denotes the time-dependent gear mesh stiffness, $x_M$ stands for the mean value of TE, $x_{fk}(t)$ represents quasi-static TE, $F_k^G$ denotes complex Fourier coefficients dependent on $\mathbf{p}$ and $\omega = 2\pi/T$ stands for basic angular frequency. Damping effects are neglected.

Gear body deflections result in imperfect gear engagement, requiring quasi-static tooth contact analysis based on the contact theory, [3]. To save a computational demand, this simulation focuses exclusively on the gear mesh, accounting for variations in the gear mesh and input torque.

The analysis is essential for evaluating both, the distribution of contact pressure and the gear mesh excitation forces, which are important for subsequent simulations. Fig. 5 shows an

example of how the load is distributed on the tooth flank, including the load path for a specific set of parameters referred to as **p.**

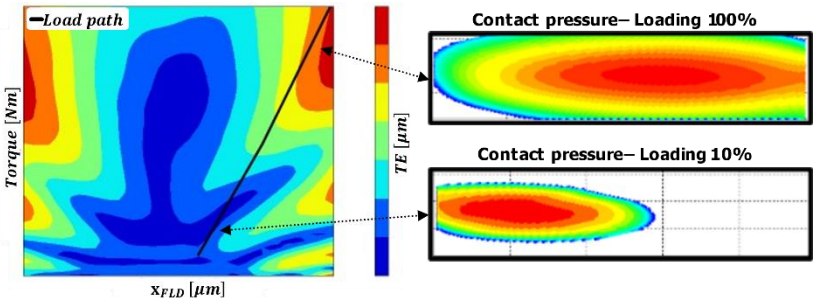


Fig. 5. (a) Example of $F_1^G$ in dependency on the gear body deflections and input torque (b) Contact pressure on gear flank for 10 % and 100 % of loading for 1 given parameter set **p**

*2.3 Linear dynamic FE analysis in the frequency domain*

The complexity of the vibroacoustic model is comparable to models from Section 2.1. Its mathematical model can be represented by the equation of motion in matrix form

$$\mathbf{M}\ddot{\mathbf{x}}(t) + \mathbf{B}\dot{\mathbf{x}}(t) + \mathbf{K}\mathbf{x}(t) = \mathbf{f}_{\boldsymbol{G}}(\mathbf{p}, t), \tag{4}$$

where $\mathbf{M}, \mathbf{B}, \mathbf{K}$ are constant linearized mass-, damping- and stiffness matrices and $\mathbf{f}_{\boldsymbol{G}}(\mathbf{p}, t)$ represents the excitation force from (3). The model linearization is based on contact linearization of non-linear model based on contact-pressure method, [4], followed by the linearization of bearings, which involves determining bearing stiffness according to the ISO 16281 standard.

Due to linearity of the system, equation (4) can be solved exclusively for unit force excitation $\mathbf{1}_{\boldsymbol{F}}$, which depends on the contact pattern results obtained from Chapter 2.2. Hence, the transfer function $\mathbf{g}(\mathbf{p}, \omega)$ can be expressed as follows

$$\mathbf{g}(\mathbf{p}, \omega) = \sum_{k=1}^{M} \frac{\boldsymbol{\phi}_{\boldsymbol{k}} \boldsymbol{\phi}_{\mathbf{k}}^{\mathbf{T}}}{\Omega_k^2 - \omega^2 + 2iD_k\Omega_k\omega} \mathbf{1}_{\boldsymbol{F}}, \tag{5}$$

where $\Omega_k$ stands for $k$-th eigenfrequency, $D_k$ represents $k$-th modal damping and $\boldsymbol{\phi}_k$ is $k$-th eigenvector. Real system response to harmonic excitation $\mathbf{f}(t)$ from equation (3) can be then reconstructed as a weighted sum of transfer function $\mathbf{g}(\mathbf{p}, \omega)$

$$\mathbf{x}(\mathbf{p}, t) = \sum_{k=1}^{N} F_k^G(\mathbf{p})\mathbf{g}(\mathbf{p}, \omega)\cos(\omega t - \psi_k), \tag{6}$$

where $\psi_k$ is phase offset for $k$-th order of gear mesh excitation.

## 3. Application

The comprehensive FE model of the electric drive system, as described in Chapter 2, comprises approx. 35 million degrees of freedom (DOFs), including 115 000 contact DOFs. The nonlinear quasi-static analysis of this model requires an average computation time of 2.5 hours.

Uncertainties arising from assembly and manufacturing process as bearing clearances, fitting clearances between components, bearing seat positions, axial pretension of bearings are covered in parameter vector **p** with 42 parameters.

In order to cover this extensive high-dimensional parameter space, the Modified Extensible Lattice Sequence method, [1], was employed, generating a total of 1300 samples that can be executed on an HPC cluster within one weekend.

An example of simulation results is presented in Fig. 6 and 7. Fig. 6a illustrates the dependency of tooth flank deviation on the deflection of the gears, as shown in (2). Fig. 7a displays the distribution of load path along with excitation orders and Fig. 7b represents the NVH system response, as elaborated in (6).

Pareto diagram is employed to identify critical factors shaping flank line deviations $\mathbf{x}_{FLD}$, as depicted in Fig. 6b. For this specific configuration, the dominant factors are bearing clearances near the gears along with the spline tolerance on the rotor shafts. In contrast, parameters such as bearing seat positions or axial pretension of bearings have minimal impact on the quality of flank line deviations $\mathbf{x}_{FLD}$.

As observed, the parameter associated with Bearing L5 exhibits a positive correlation, whereas Bearing L2 demonstrates a negative correlation. From this, it can be inferred that the values for the Bearing L5 parameter should be increased, while the values for Bearing L2 should be decreased.

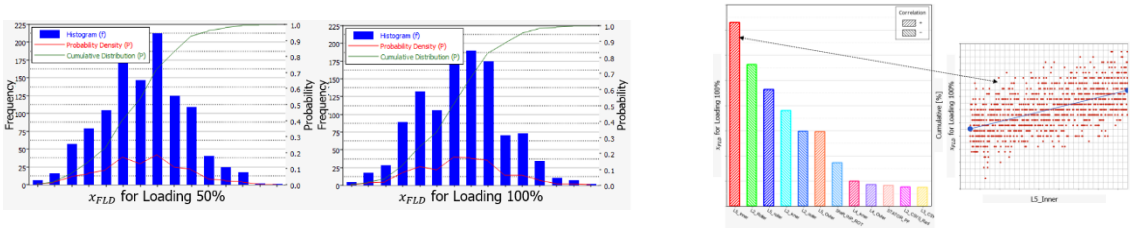


Fig. 6. (a) Histograms of flank line deviations $\mathbf{x}_{FLD}$ for different load levels (b) Pareto diagram of flank line deviations $\mathbf{x}_{FLD}$ for loading 100 % along with scatter plot of parameter L5_inner with a positive linear trend

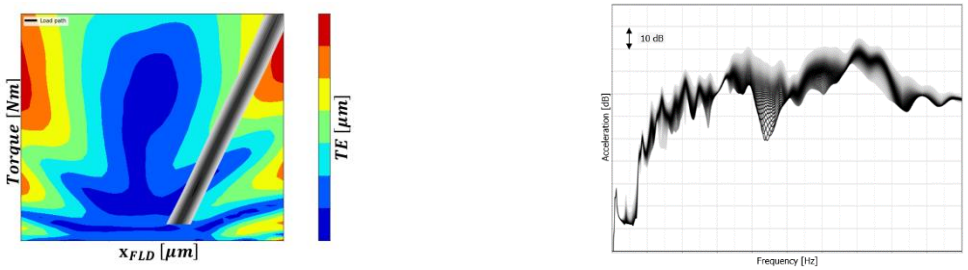


Fig. 7. (a) Load path distribution together with probability distribution of the gear tilting (b) An example illustrating the propagation of system response-induced structure-borne noise, assessed within coupling positions to the car frame, arising from variations in gear mesh excitation


## Acknowledgements

The authors thank to ZF management for supporting their participation in the conference and in preparing this paper.


## References


[1] Altair HyperStudy, https://2021.help.altair.com/2021/hwdesktop/hst/topics/design_exploration/methods_doe_r-1.htm.
[2] Börner, J., Noise excitation caused by gears, ZF internal material, 2017.
[3] Fuentes, A., Litvin, F. L., Gear geometry and applied theory, Cambridge University Press, Cambridge, 2004.
[4] PERMAS, User's Reference Manual 450 v19, INTES Publication, Stuttgart, 2022.